Egyptian Journal of Chemistry

http://ejchem.journals.ekb.eg/

Fabrication and Study of ZnO thin Films using Thermal Evaporation Technique

Ghuzlan Sarhan Ahmed*, Tahir Hamad Mahmoud, Hanaa Ibraheem Mohammed, Aeshah Ali Hussein

Department of Physics, College of Education for Pure Science, Ibn Al-Haitham, University of Baghdad, Baghdad, Iraq.

Abstract

In this study, thin film Zinc oxide (ZnO) deposited by thermal evaporation techniques on unheated glass substrates. The findings of X-ray diffraction (XRD) show that the ZnO films are amorphous before annealing. The subsequent diffraction patterns demonstrate that the films crystalline into polycrystalline mixed Tetragonal α-ZnO compounds and Orthorhombic ß-ZnO compounds. Atomic power microscope (AFM) shows that the ZnO films are of a large homogeneous surface. The median crystallite size is calculated from XRD data, which are increased for all thickness with an increasing ringing temperature and are less than the AFM data. The findings of the optical properties show that with rising annealing temperature for all thicknesses, the transmittance decreases. ZnO film shows transmittance that exceeds 95% in the IR radiation area of the spectrum at the lower thickness of 60 nm annealed at 523 K for 2 hr, but decreases to 87% percent with increasing annealing temperatures, although ZnO films with thicknesses of 130 nm annealed at 723 K for 2 hr have a transmittance of 94 % and 88 % in the IR region, but decreases High transmission in the IR area reveals that ZnO films are good materials for agricultural applications. All the prepared ZnO-thin films were n-type semiconductors and it is known that the concentration of the carriers (n) and the conductivity (σ) increased with an ever-greater annealing temperature, while their mobility (μ) and resistivity (ρ) is reduced with an increase in the annealing temperature.

Keywords: Type your keywords here, separated by semicolons ;

1. Introduction

Since the microelectronic solid-state devices are all based on substrate structures produced by deposition techniques, thin film deposition technology may well be considered as the main key to the advancement of devices such as computers. Excellent stability and precision of electronic devices is the characteristic feature of thin film technology [1].

In the 20th century, advances in thin film deposition processes have led to a number of technical accomplishments in the fields of magnet media, semiconductor instruments, LEDs, visual lacquering (anti-reflective lacquers), rugged tool lacquers and for both the production of electricity (thin film solar cell) and storage (thin-film batteries). It is also used for medical products by the supply of thin films. A multilayer stack of thin films is termed [2].

Several research groups have already focused on the semiconductor zinc oxide (ZnO). ZnO has been used in many applications like transducers piezoelectric, emitters of UV, sensors of gas, and for solar cells owing to their bulk availability, single crystal structure, and high exciton binding energy (60 MeV). ZnO is very promising for optoelectronics as a host of UV light [3,4] since it has a large bandgap (3.27 eV at room temperature). In addition, using an artificial light source, ZnO has been used as an organic photocatalyst for water purification [5-7].

High-quality ZnO films have been produced using pulsed laser deposition (PLD), molecular beam epitaxy (MBE), and chemical vapor deposition (CVD) anodizing, sputtering, and thermal evaporation [3,4,8-13]. Deposition of thermal oxidation has gained very little consideration from study groups considering its apparent financial and simplicity [14-17].

*Corresponding author e-mail: ghzlan82sn@gmail.com : Tel (+9647902762882)
Receive Date: 05 April 2021, Revise Date: 16 April 2021, Accept Date: 27 April 2021
DOI: 10.21608/EJCHEM.2021.71184.3563
©2021 National Information and Documentation Center (NIDOC)

Furthermore, no photocatalytic studies on polycrystalline ZnO films deposited at low temperatures using this process have been performed to our knowledge.

The effect of ionizing radiation on the properties of the nanocomposites (PVA-PAA-Al_2O_3) by means of gamma irradiation on were studied by H.S. Rashed et al. [18].

The percentage effect of the oxygen on the ZnO films' structural and morphological properties has been studied by S. N. Fatimah et al. [19] by thermal evaporation at 900 °C of pure zinc under the flow of varying percentages of argon and oxygen gases.

Hassan and Hashim developed high-quality ZnO nanostructures at room temperature using a basic vacuum thermal evaporator constructed from metallic Zn powders (99.999 % purity) on a silicon (100) substructure [20]. They argued that the time is a critical factor for their synthesis.

The physical properties of the PEG polymer dissolved in distilled water for different concentrations have been analyzed by H.S. Rasheed [21]. The studied properties were found to be linearly dependent with the increase of PEG concentrations.

A pure nanostructured thin films zinc oxide (ZnO) were prepared by M. Obaida *et al.*[22] using a simple pulsed spray pyrsolysis (PSP) technique at different deposition temperatures and spraying times on glass substrates. The XRD measurements showed that the polycrystalline ZnO hexagonal wurtzite phase was found to be preferably oriented perpendicular through c-axis along (002) plane.

S. Abd Alhalim et al. [23] filled the cotton fabric with nanoparticles of zinc oxide in situ. As a dispersion medium, urea was used to convert zinc acetate salt into ZnONPs within the cotton fabric matrix. They determined the effect of in situ loaded ZnONPs on the thermal behavior, chemical integrity, microstructure, mechanical properties and air permeability (percent) properties of the cotton fabrics, these cotton. It was observed that the physical properties of the ZnONPs loaded in situ were dependent on the concentration of the ZnONPs. Biomedical uses are recommended for these treated cotton fabrics.

Pb-doped ZnO nanotube films on Si (100) substrate is prepared using a simple thermal evaporation technique. The element's contents were investigated using X-ray photoelectron spectroscopy (XPS) and energy-dispersive X-ray spectroscopy (EDX), which revealed the existence of a stoichiometry ZnO nanotube film. The XRD pattern revealed the wurtzite step of ZnO as well as a polycrystalline structure. Using scanning electron microscopy (SEM) images, the thickness and morphology of the films is investigated from cross sections of the films and the base by B. Abdullah et al. [24].

The effect of annealing temperature on structural, optical, electrical, and mechanical properties of various samples based on ZnO-Mg (MZO) thin films has been studied by F. Lekoui[25]. Their tested samples were annealed at 300, 400, and 500 °C at ambient pressure, while the control samples were left unannealed. At 300 °C, X-ray diffraction (XRD) study confirmed the growth of the ZnO hexagonal wurtzite structure, while at 500 °C, the structure crystallinity increased. The presence of Zn, O, and Mg elements is shown by electron-dispersive spectroscopy (EDS) review. For both samples, Raman spectroscopy shows the presence of A1(LO) and LVM modes.

This paper focus on studying the photocatalytic, growth and behavior of thin films of ZnO prepared by vapor deposition of thermal technique. The properties of the films deposited, the chemical composition, crystal structure, and the morphology of the surface are all investigated. The photocatalytic activity of films deposited on unheated, thoroughly cleaned glass substrates is studied, and the results are described.

2. Materials and Methods

The substance used in this work is zinc oxide (ZnO) with a high purity (99.9%), white solid and density of 5.606 g/cm^3, as a powder material taken from Riedel-de Haën in Germany.

A glass substrate was used to deposit thin films by thermal evaporation technique has $(2.54 \times 7.62)\ cm^2$ and 0.1 cm thickness.

It is really important to clean the substrate because it has a great effect on the properties of the thin films, therefore, the following steps were done.

1. In a clean beaker containing distilled water, the glass slides were immersed and then rinsed in an Ultrasonic for (15mins).
2. The substrates cleaned by alcohol.
3. The substrates are dried for 15 minutes by thermal oven or drying the slides by cleaning them later with soft paper that they can be ready to use in the deposition process.

Setting the distance between the substrate and the source to 6 cm produced the ZnO film. In the evacuated deposition chamber, the base pressure is set to 10^{-7} mbar. The source current has been gradually increased (up to 3 A), and vapor species have been concentrated onto glass substrates. Following deposition, these films were thermally oxidized in the air using the Linn High Therm GmbH furnace (Model LM 312) at temperatures ranging from 200 to 500 °C for a time period of 2 hours. The diffraction of x-ray method was used to characterize the films' structural properties (ray $K_{\alpha 1}$ of Cu, $\lambda = 1.5406$ Å). The thickness of the films was calculated by Dektak profilometry.

Results and Discussion

3.1 Structural and Morphological Properties
3.1.1 X– Ray diffraction analysis

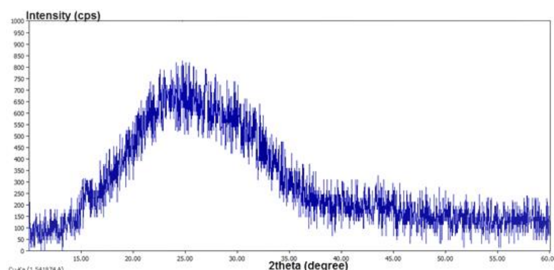

The X-Ray diffraction (XRD) study is conducted using Cuka radiation (λ=1.5406 Å) with an operating voltage of 15 kV and a current of 30 mA for the prepared ZnO thin films. XRD peaks are reported at RT between 0º-60º. The structural investigation shows that the lead oxide films are in an amorphous state until annealing (i.e., no diffraction peaks have been observed), as seen in Figure 1.
In determining the composition of lead oxide thin films deposited on unheated glass substrates, heat treatment plays an important role.

Figure 1. Diffraction spectrum at thickness t=130 nm of deposited ZnO thin film before annealing.

Figures 2, 3 demonstrated the XRD pattern of ZnO thin films, compounds with annealing temperature of 523, 623 and 723 K for thicknesses reliably around 60nm and 130nm respectively. The composition of all films is polycrystalline, according to the Joint Committee of the Powder Diffraction Standard (JCPDS).

The XRD pattern analysis reveals more distinct and dense diffraction peaks for the ZnO film prepared with 60nm thickness and annealed at 523K as shown in Figure(2.a), while the small and narrow peaks superimposed on the broad backdrop of the amorphous portion of the glass substrate as shown in Fig. (2.b and c) are further increased to 623 K and 723 K when the annealing temperature is increased.

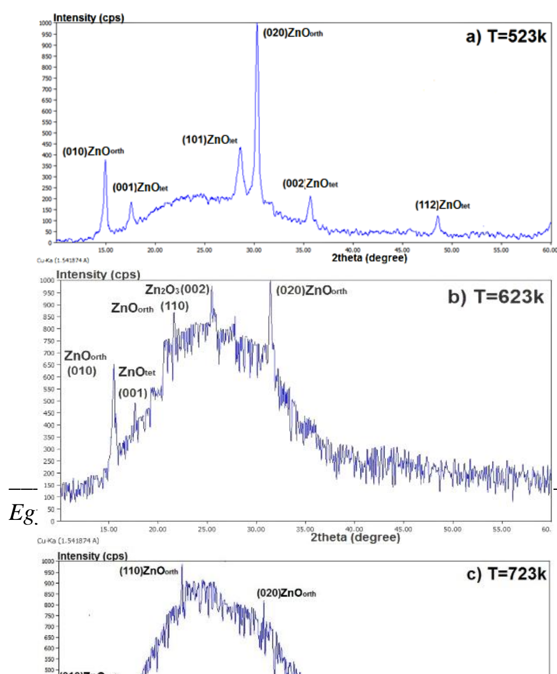

Figure 2. Diffraction spectrum of ZnO films deposited at thickness t=60nm and exposed to various annealing temperatures.

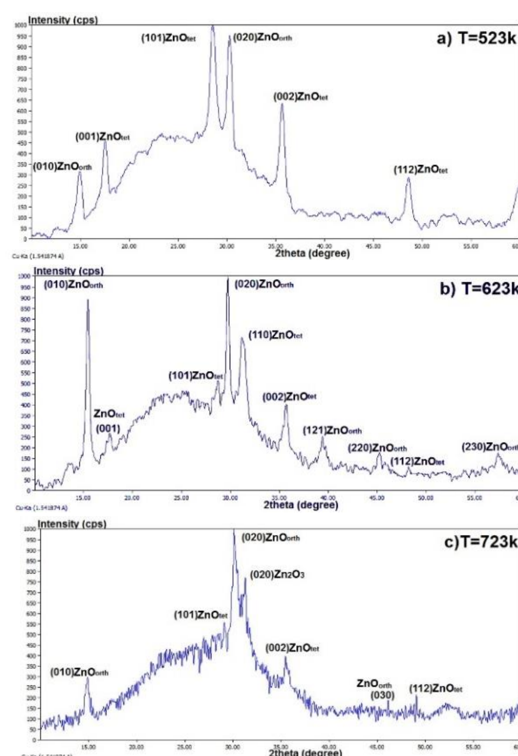

Figure 2. Diffraction spectrum of ZnO films deposited at thickness t=130nm and exposed to various annealing temperatures.

3.1.2 The Microscope of the Atomic Force (AFM)

The AFM in tapping mode is used to analyze the surface morphology of thin ZnO films in compliance with the annealing temperatures. Figures (3-9) shows the standard double-dimensional diagrams and the distribution map of the growth granular divisions on the surfaces of the deposited ZnO thin films with clear thicknesses of 60nm and 130nm and for the temperatures 524K, 623K and 723K.

The white regions reflect the shape of aggregated grains above each other in Figs. (3-9). We may assume that in these areas, adjacent grains producing large clusters are mixed. In the white area's grains are therefore bigger than in other regions. The mechanism of film growth is thought to have first evolved layer by

layer and then island type of growth from these observations.

All ZnO thin films show a uniform granular surface morphology, and it can be shown that the grains are distributed over the glass substrates evenly without any cracks. With increasing rubbish temperature at 523 K, 623 K and 723 K values in the same spacing as with increasing thickness at values between 60nm and 130nm are improved film roughness and medium square (RMS) values.

The increase in RMS contributes to a more than horizontal increase in crystalline growth in the vertical direction. The film crystallites are wider and the surface roughness and surface thickness are higher as a result. The surface thickness rate value reflects the thickness of the roughness of the film surface, which accounts for the largest granular crystalline tops on the surface.

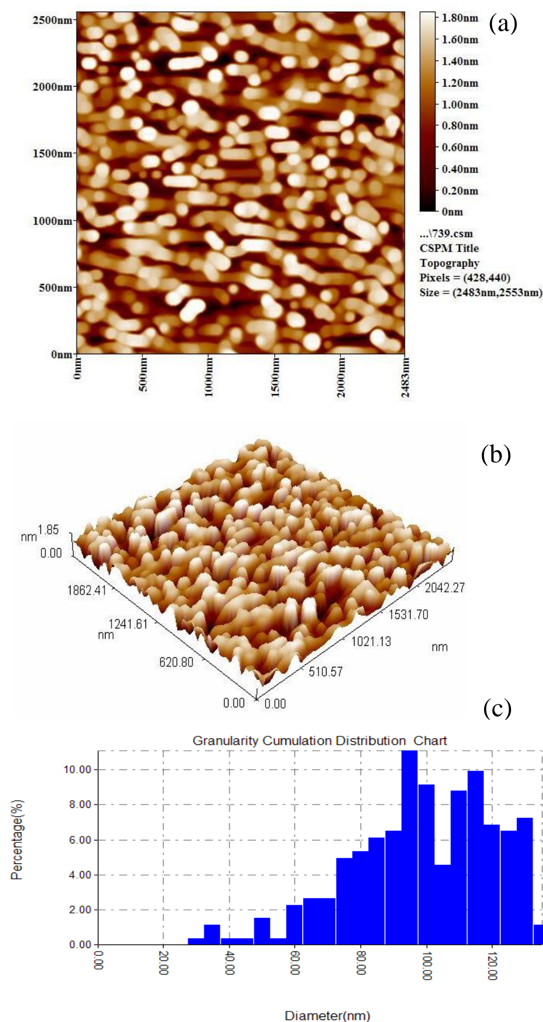

Figure 3. AFM of ZnO thin film surface morphology prepared at 60nm thickness with 523K a) 2-D, b) 3-D annealing temperature, and c) distribution of granularity.

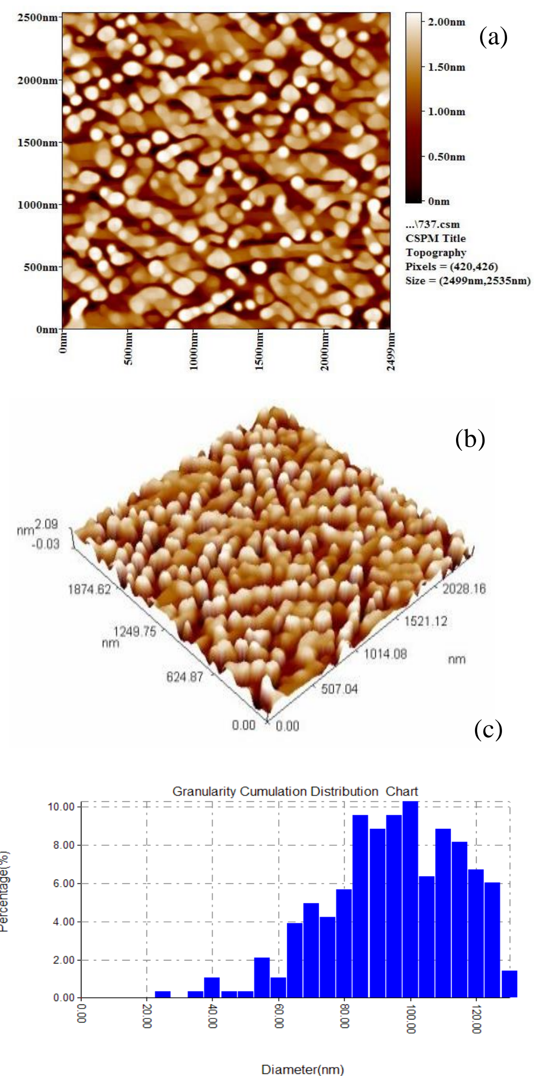

Figure 3. AFM of ZnO thin film surface morphology prepared at 60nm thickness with 623K a) 2-D, b) 3-D annealing temperature, and c) distribution of granularity.

3.2 Optical Properties

The optical properties of ZnO thin films were studied by studying the absorbance spectrum, these properties are transmittance (T), reflectance(R), optical energy gap (E_g), absorption coefficient (α), extinction coefficient (k_o), real and imaginary dielectric constant (ε_r, ε_i), and the refractive index (n),

3.2.1 Transmittance(T)

Figures 7 and 8 shows the variation of the transmittance (T) versus the wavelength for ZnO thin films for 60nm and 130nm thickness with three different annealing temperatures 523K, 623K and 723 K. Advantageous features of ZnO thin films are good optical transmission for wavelengths greater than 400

nm in the visible region, which is one of the prerequisites for opto-electronic applications, especially for solar cell window layers, because it acts as a filter and anti-reflection coating, minimizing the energy loss in the incident radiation to its minimum value. The high transmittance in the IR radiation region also means that ZnO films are suitable materials in temperate regions and in agriculture for warming use in homes.

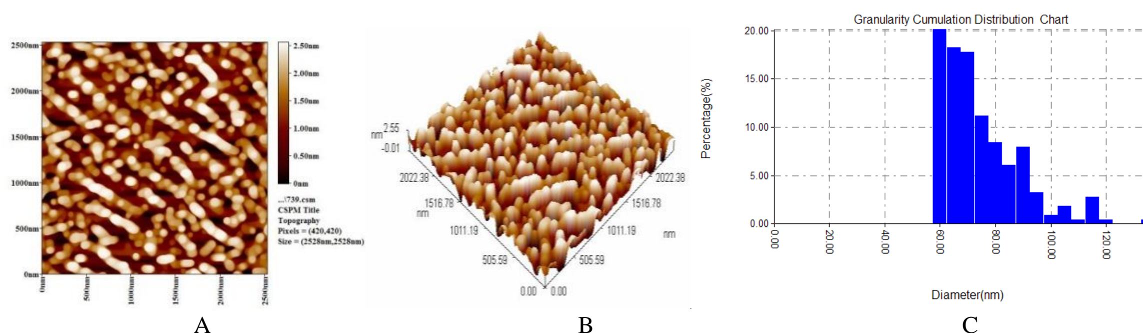

A B C

Figure 3. AFM of ZnO thin film surface morphology prepared at 60nm thickness with 723K a) 2-D, b) 3-D annealing temperature, and c) distribution of granularity.

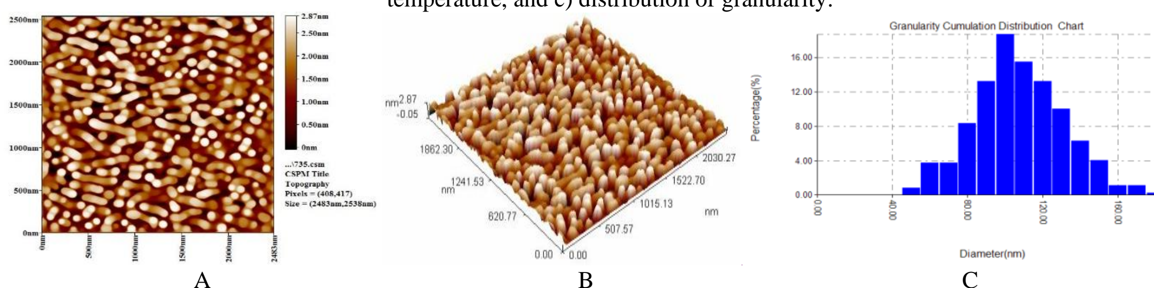

A B C

Figure 4. AFM of ZnO thin film surface morphology prepared at 130nm thickness with 523K a) 2-D, b) 3-D annealing temperature, and c) distribution of granularity.

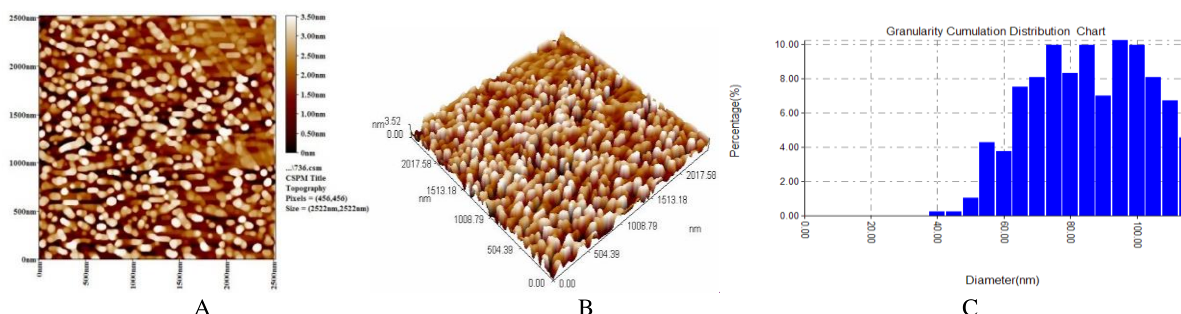

A B C

Figure 5. AFM of ZnO thin film surface morphology prepared at 130nm thickness with 623K a) 2-D, b) 3-D annealing temperature, and c) distribution of granularity.

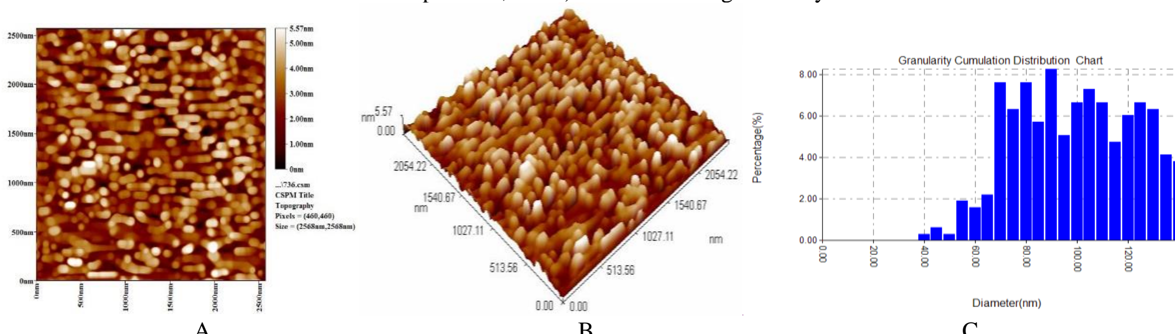

A B C

Figure 6. AFM of ZnO thin film surface morphology prepared at 130nm thickness with 723K a) 2-D, b) 3-D annealing temperature, and c) distribution of granularity.

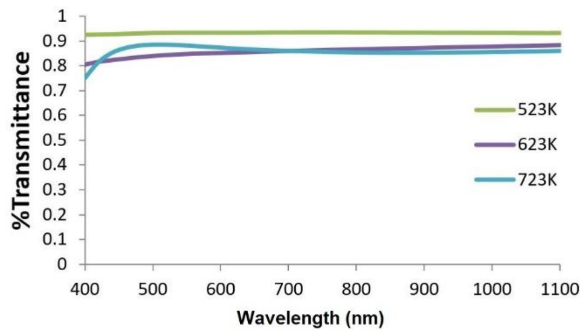

Figure 8. Transmittance spectra as a function of the wavelength at various annealing temperatures of ZnO thin films at 60nm thickness.

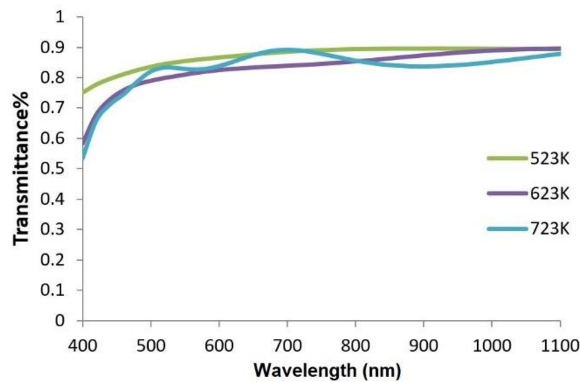

Figure 9. Transmittance spectra as a function of the wavelength at various annealing temperatures of ZnO thin films at 130nm thickness.

3.2.2 Absorbance (A)

The optical absorbance of ZnO thin films as function of wavelength studied at 60nm and 130 nm thin film thicknesses are shown in Figs. 10 and 11, respectively.

In the lower wavelength region (ultraviolet region), where the film is extremely absorbent, the optical absorbance for the studied samples decreases with increasing wavelength (VIS and IR regions). The findings show that as the temperature of annealing is increased, the absorbance increases and has less absorbance at 523K, whereas at 723K it has the maximum absorbance for different thicknesses. In both ZnO thin films, a red change (higher wavelength side) is noted in the absorption edge towards the lower band difference.

3.2.3 The coefficient of absorption (α)

The absorption coefficient is determined from the area of strong absorption at the film's fundamental absorption edge. Variation of the absorption coefficient versus the energy of incident radiation (hν) of thin films of ZnO with various thicknesses consistently 60nm and130nm for 2 hour annealing temperatures of 523 K, 623 K and 723K as seen in Figs. 12 and 13, respectively.

The absorption coefficient is increased for each of the studied thicknesses with the increased annealing temperature for the entire measurement spectrum. The coefficient of absorption has high values ($\alpha > 0.4\ cm^{-1}$), which means that the likelihood of a direct transition.

3.2.4 Optical Energy Gap (E_g^{opt})

Figures 14 and 15, shows the experimental values of $(\alpha h\nu)^2$ reliably plotted against photon energy (hν) of ZnO thin films for various thicknesses of 60 nm and 130 nm with annealing temperatures of 523 K, 623 K and 723K at 2 hr.

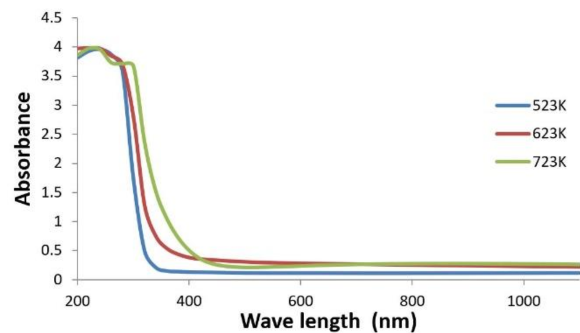

Figure 10. Absorption spectra as a function of the wavelength at various temperatures of ZnO thin films with a thickness of 60nm.

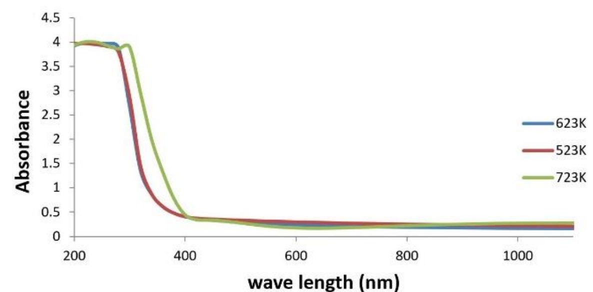

Figure 11. Absorption spectra as a function of the wavelength at various temperatures of ZnO thin films with a thickness of 130nm.

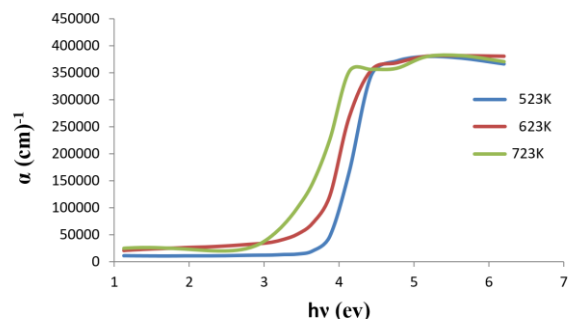

Figure 12. The photon energy (hν) vs. absorption coefficient for 60 nm of thin films ZnO at different temperatures.

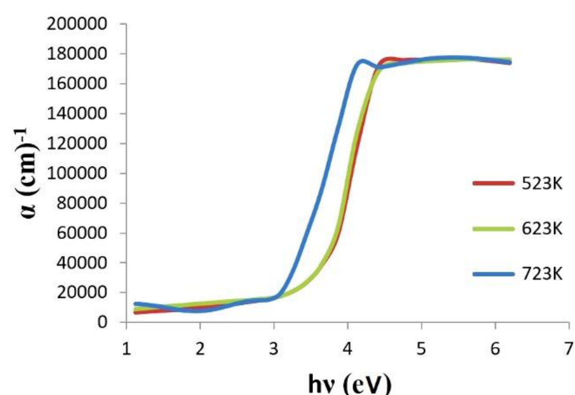

Figure 13. Absorption coefficient and photon energy (hν) of 130 nm ZnO thin films at different temperatures.

The optical energy gap E_g^{opt} is calculated using the photon energy axis as the intercept of the extrapolated linear component of the curve (hυ) at $(\alpha h\nu)^n = 0$. The linear nature of the plots at the absorption edge confirmed that all deposited films are direct transition type semiconductors.

The value of optical energy gap which are determined for ZnO thin films at $(\alpha h\nu)^2=0$, are equal to (3.79, 3.60, and 3.490 eV), (3.520, 3.320, and 3.140 eV) for different thicknesses 60 nm, 130 nm for the annealing temperatures 523K, 623K and 723K, respectively.

3.2.5 The index of refraction (n)

In the range 300-1100 nm, the refractive index varies with wavelength is consistent for different thicknesses at 60nm and 130nm with annealing temperature at 2 hours 523 K,623 K and 723 K, as was investigated and analyzed in Figs. 16 and 17.

As the wavelength increases, the refractive index increases to maximal values in the region of the ultraviolet spectrum and then starts to decline. The refractive index also increases with the rise in annealing temperature at higher wavelengths and a decrease in low wavelengths with various thicknesses in both samples. The explanation is because of the films' reflectivity and optical energy gap. The difference in the value of the refractive index is related to packing density and the rise in crystalline growth and further orientation.

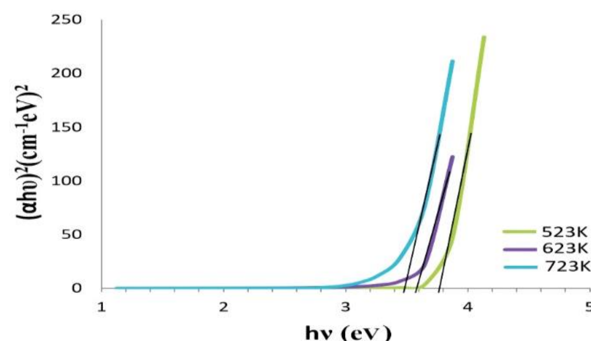

Figure 14. The photon energy (hν) v.s $(\alpha h\upsilon)^2$ of thin films ZnO for 60 nm thickness at different temperature.

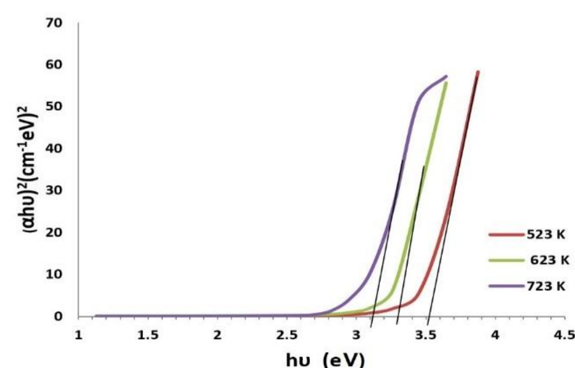

Figure 15. Shows the relation between photon energy (hν) and $(\alpha h\upsilon)^2$ for ZnO thin films for 130 nm thickness at different temperature.

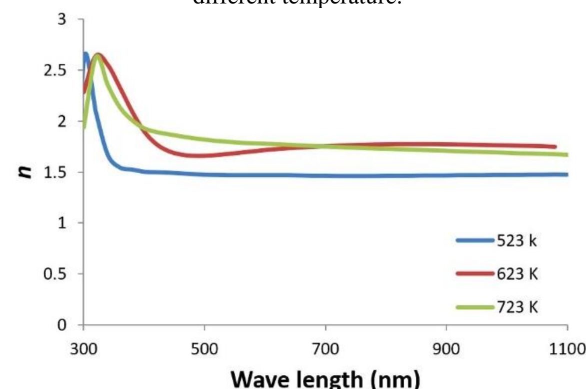

Figure 16. The relation between the index of refraction and the wavelength for films ZnO at thickness 60 nm.

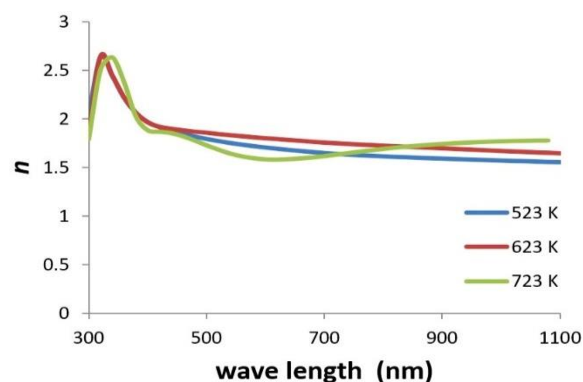

Figure 17. The relation between the wavelength and the refractive index for ZnO films at thickness 130 nm.

3.2.6 Extinction Coefficient (K_o)

Figures (18) and (19) display the variation of the extinction coefficient with respect to the wavelength in the 200-1100 nm range of thin ZnO films for various thicknesses reliably 60nm and 130nm with 523 K, 623 K and 723K annealing temperature at 2 hours. It can be shown from the figures that the behavior of the extinction coefficient is close to the curve of the absorption coefficient because of its similarity to the above relationship.

On both of the measuring ranges for the two thicknesses studied, the extinction coefficient increased with rising annealing temperature, and even the abrupt rise in the extinction coefficient was on the verge of absorption. These findings may be attributed both to increasing absorption due to the transmission phase and to increasing scattering due to an increase in RMS.

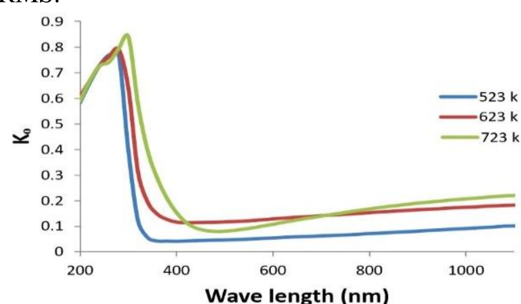

Figure 18. The relation between wavelength and the Extinction Coefficient (K_o) for ZnO films at thickness 60 nm.

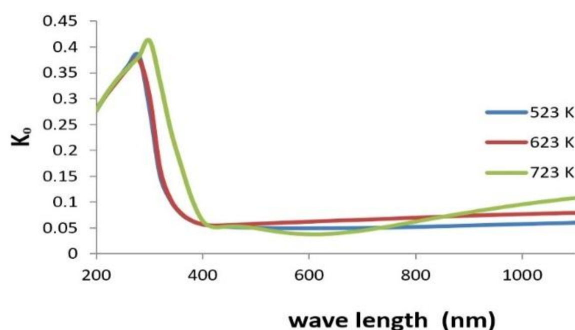

Figure 19. The relation between the Extinction Coefficient (K_o) and the wavelength for ZnO films at thickness 130 nm.

3.2.7 The Constants of Dielectric (ε_r and ε_i)

Figures (20) and (21) shows the variation of the dielectric constants for real and imaginary parts (ε_r and ε_i) with wavelength for 60 nm and 130 nm thickness of ZnO, respectively.

The real part is how long light will delay in the material, while the imaginary part is how a dielectric energy from a dipole motion absorbs an energy. The standard dielectric constant is represented by the real component, while the free energy radiation absorption is represented by the imaginary part.

In general, both ε_r and ε_i increase as the annealing temperature rises. The numbers show that the actual part's values are higher than the fictional part's and that they follow a similar trend.

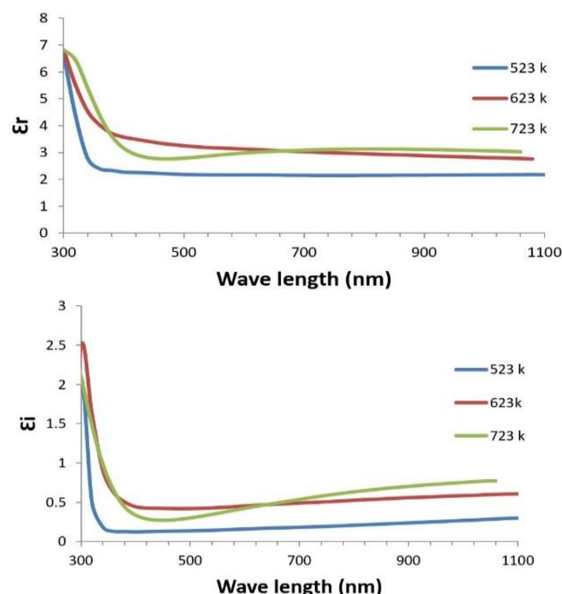

Figure 20. The relation between the Dielectric Constants (ε_r and ε_i) and the wavelength for ZnO films at thickness 60 nm.

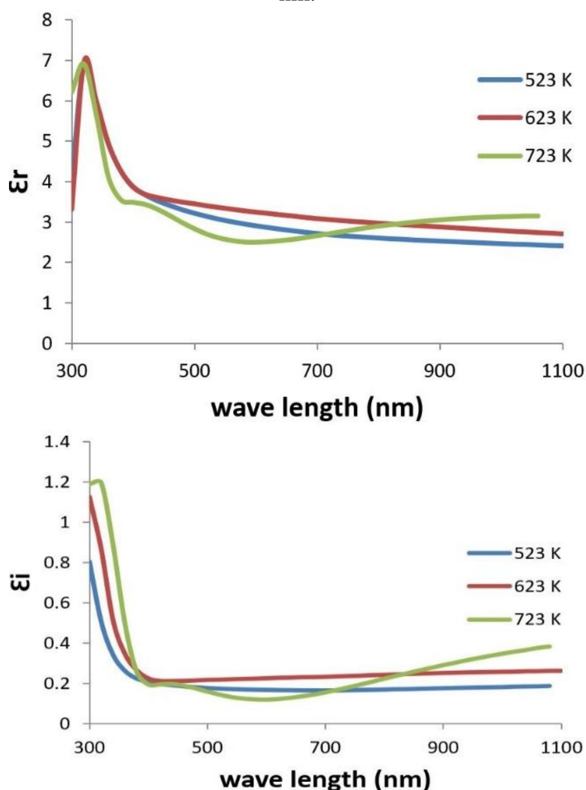

Figure 21. The relation between the constants of dielectric (ε_r and ε_i) and the wavelength for ZnO films at thickness 130 nm.

3.2.8 Optical Conductivity ($\sigma_{opt.}$)

The variation of the optical conductivity ($\sigma_{opt.}$) with the wavelgnth for thicknesses 60nm and 130 nm for ZnO thin films annealed at three different temprattures 523 K, 623 K and 723 K are shown in Figs. (22) and (23).

From these figures, it can be seen that the optical conductivity increases steadily in the low energy region, while the value of the optical conductivity increases dramatically in the high energy region (near the absorption edge), while the annealing temperature increases within the same thickness. This may be attributed to the change in crystallinity due to the increase in charge carrier concentration. The variation in optical conductivity varies in a similar way as the variation of the imaginary component of dielectric constant, since σ_{opt} depends on imaginary part.

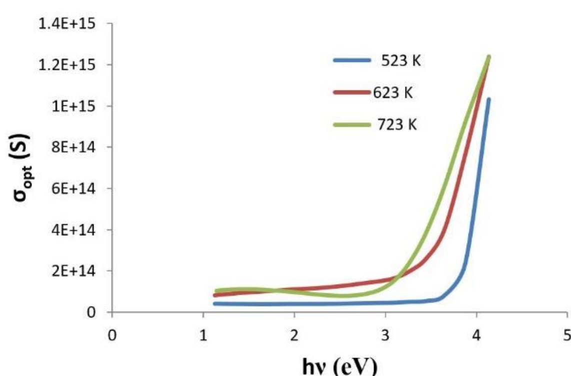

Figure 22. The relation of the photon energy and the optical conductivity ($\sigma_{opt.}$) for the the thins sfilms ZnO at thickness 60 nm.

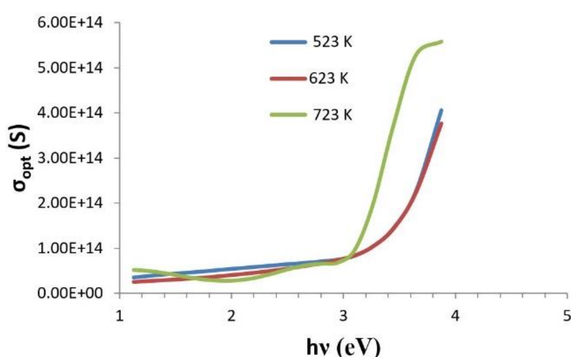

Figure 23. The relation of the Conductivity of the optical ($\sigma_{opt.}$) and the energy of the photon for thin films ZnO at thickness 130 nm.

4. Conclusions

In the visible and IR radiation regions of the spectrum, ZnO films at the lower thickness of 60nm annealed at 523K have a higher transmittance that reaches 93%, but decreases with increasing annealing temperatures. In the visible and IR radiation region, high transmission means that ZnO films are suitable materials for the solar cell window and gas sensor industry, as well as for the application of heating in homes and in agriculture.

5. References

[1] K. L. Chopra, "Thin film devices application", Plenum press, New York, (1983).
[2] S. M. Ahmed, L. A. Latif, and A. K H. Salim, J Basrah Res, Vol.37 (2011) 57.
[3] J. Liqianga, S. Xiaojunb, S. Jingc, C. Weiminb, X. Zilic, D. Yaoguoc, F. Hongganga, Sol. Energy Mater. Sol. C 79 (2003) 133.
[4] S. Chakrabarti, B.K. Dutta, J. Hazard. Mater. B 112 (2004) 269.
[5] S. Rabindranathan, S. Devipriya, S. Yesodharan, J. Hazard. Mater. B102 (2003) 217.
[6] D. Chen, A.K. Ray, Chem. Eng. Sci. 56 (2001) 1561.
[7] K. Tennakone, J. Bandara, Appl. Catal. A: Chem. 208 (2001) 335.
[8] S.-S. Lin, J.-L. Huang, Surf. Coat. Technol. 185 (2004) 222.
[9] Ya.I. Alivov, A.V. Chernykh, M.V. Chukichev, R.Y. Korotkov, Thin Solid Films 473 (2005) 241.
[10] A.Kh. Abduev, B.M. Ataev, A.M. Bagamadova, Inorg. Mater. 11 (1987) 1928.
[11] S. Choopun, H. Tabata, T. Kawai, J. Cryst. Growth 274 (2005) 167.
[12] Y. Chen, D.M. Bagnall, H. Koh, K. Park, K. Hiraga, Z. Zhu, T. Yao, J. Appl. Phys. 84 (1998) 3912.
[13] Y. Yamaguchi, M. Yamazaki, S. Yoshihara, T. Shirakashi, J. Electroanal. Chem. 442 (1998) 1.
[14] S.J. Chen, Y.C. Liu, J.G. Ma, D.X. Zhao, Z.Z. Zhi, Y.M. Lu, J.Y.
[15] Zhang, D.Z. Shen, X.W. Fan, J. Cryst. Growth 240 (2002) 467.
[16] R.K. Gupta, N. Sridhar, M. Katiar, Mater. Sci. Semicond. Process. 5 (2002) 11.
[17] Y.G. Wang, S.P. Lau, H.W. Lee, S.F. Yu, B.K. Tay, X.H. Zhang, H.H. Hng, J. Appl. Phys. 94 (2003) 354.
[18] Hiba S. Rasheed, Israa A. Abbas, Ameera J. Kadhum, and Hiyam Ch. Maged, AIP Conference Proceedings 2190, (2019) 020013.
[19] S. N. Fatimah Hasim, M. A. Abdul Hamid, R. Shamsudin, A. Jalar, J. Phys. Chem. Sol. 70 (2009) 1501.
[20] N. K. Hassan and M. R. Hashim, Sains Malaysiana 42(2)(2013) 193.
[21] H. S. Rasheed, Physics AUC, 29 (2019) 36.
[22] M. Obaida, I. Moussa, S. A. Hassan, H. H. Afify and A. Abouelsayed, Egypt. J. Chem. Vol. 63 (2020) 233.
[23] S. Abd Alhalim, M. Mabroukorcid, S. K. Ibrahim, N. H. Hamdy, A. Ramadan, Egypt. J. Chem. Vol. 63(2) (2020) 625.
[24] B. Abdallah, M. Kakhia, and Asmahan Obaide, Plasmonics, (2021): doi: https://doi.org/10.1007/s11468-021-01420-x
[25] F. Lekoui, S. Hassani, M. Ouchabane, H. Akkari, D. Dergham, W. Filali, and E Garoudja, Braz. J. Phys. (2021) :doi: https://doi.org/10.1007/s13538-021-00866-y